NJC

PAPER

View Article Online
View Journal | View Issue

Cite this: *New J. Chem.*, 2014, **38**, 5324

Flowerlike Bi_2S_3 microspheres: facile synthesis and application in the catalytic reduction of 4-nitroaniline

Fan Guo, Yonghong Ni,* Yue Ma, Nannan Xiang and Chang Liu

Received (in Porto Alegre, Brazil) 3rd June 2014,
Accepted 15th August 2014

DOI: 10.1039/c4nj00900b

www.rsc.org/njc

Flowerlike Bi_2S_3 microspheres have been successfully synthesized *via* a facile wet chemical route in air at 110 °C for 10 min, employing bismuth nitrate and thiourea in a molar ratio of 1 : 2 as the starting reactants, ethylene glycol as the reaction medium and polyvinylpyrrolidone (PVP) as the structure-directing reagent. Electron microscopy observations showed that the as-obtained product looked like an Asteraceae plant called *Echinops Sphaerocephalus Linn* in nature. The N_2 sorption–desorption experiments showed that the Brunauer–Emmett–Teller (BET) area of the flowerlike microspheres was 32.4 m^2 g^{-1}. Some factors influencing the formation of flowerlike Bi_2S_3 microspheres were investigated, including the reaction temperature, and the sort and amount of the surfactant. The experiments showed that the Bi_2S_3 micro/nanostructures prepared in the present work could be used as new-type catalysts for the reduction of some aromatic nitro compounds, such as 4-nitroaniline, 2-nitrophenol and 4-nitrophenol. It was found that the as-obtained flowerlike Bi_2S_3 microspheres contributed to the best catalytic activity.

1. Introduction

Over the past two decades, nanostructural metal chalcogenide semiconductors have been receiving extensive research interest due to their excellent physicochemical properties and promising applications in many fields, including solar cells, light-emitting diodes, sensors, thermoelectric devices, fuel cells and nonvolatile memory devices.[1–4] Among them, Bi_2S_3, an important member of the family of the main group of metal chalcogenides $A_2^{V}B_3^{VI}$ (A: As, Sb, and Bi; B: S, Se, and Te), has always been paid much attention owing to its lamellar structure and direct band-gap of 1.2–1.7 eV,[5,6] as well as numerous applications in photovoltaics,[7] thermoelectrics[8] and X-ray computed tomography.[9]

In recent years, Bi_2S_3 nanostructures were found to exhibit some new properties or applications, including the photoresponse and field emission property,[10] the electrochemical hydrogen storage capacity,[11,12] photocatalytic activity,[13–15] and as an electrode material in lithium ion battery.[16] For instance, Yu *et al.* prepared elegant Bi_2S_3 nanoflowers through the vapor deposition technology at 650 °C for 2 h and investigated the photoresponse and field emission property of the as-obtained nanoflowers.[17] Zhang and coworkers studied the electrochemical hydrogen storage capacity of Bi_2S_3 flowerlike patterns constructed by abundant nanorods, which were synthesized by an L-cysteine-assisted hydrothermal route.[11] Chen *et al.* fabricated hierarchical Bi_2S_3 nanostructures *via* a thioglycolic acid assisted wet chemical route at 100 °C for 6 h,[14] and investigated the photocatalytic activity of the as-prepared hierarchical nanostructures. In the presence of 10 mg of the as-prepared hierarchical nanostructures, ~97% of methyl orange dye with the original concentration of 10 mg L^{-1} could be degraded by the UV irradiation for 4 h. Ma and coworkers hydrothermally synthesized Bi_2S_3 nanostructures of various shapes at 180 °C for 12 h by varying the original sulfur ion source, and investigated the Li intercalation/deintercalation performances of the as-obtained nanostructures with various shapes.[16] However, the above methods usually require high temperature, long time and even a series of complicated procedures. Obviously, it is still necessary and significant to develop a facile and efficient approach for the large fabrication of uniform Bi_2S_3 micro-/nanostructures and explore new properties and applications.

Recently, the catalytic reduction of certain aromatic nitrocompounds in excess $NaBH_4$ solution has attracted much attention since the reductive product has wide applications in industry.[17] More importantly, this reduction reaction has become one of the model reactions for evaluating the catalytic activity of various free or immobilized inorganic nanoparticles in aqueous solutions, including noble metal, Ni, TiO_2, Ni–Co alloys, Ni–NiO, and Ni–Ni_xP_y nanocomposites.[18–23] In this paper,

College of Chemistry and Materials Science, Key Laboratory of Functional Molecular Solids of Education Ministry, Anhui Laboratory of Molecule-Based Materials, Anhui Key Laboratory of Functional Molecular Solids, Annuli Normal University, 1 Beijing East Road, Wuhu, 241000, PR China.
E-mail: niyh@mail.ahnu.edu.cn; Fax: +86-553-3869303

we designed a simple wet chemical route for the fast preparation of uniform flowerlike Bi_2S_3 microspheres. Bismuth nitrate and thiourea in a molar ratio of 1 : 2 were used as the starting reactants. Flowerlike Bi_2S_3 microspheres were obtained in an ethylene glycol system containing polyvinylpyrrolidone (PVP) in air at 110 °C for 10 min. Our interest mainly focused on the application of Bi_2S_3 as a new-type of catalyst for the reduction of some aromatic nitro compounds in an excess $NaBH_4$ aqueous system.

2. Experimental section

All reagents and chemicals were analytically pure, bought from Sinopharm Chemical Company, and used without further purification.

2.1 Preparation of flowerlike Bi_2S_3 microspheres

In a typical procedure, 0.8 mmol (388 mg) of $Bi(NO_3)_3{\cdot}5H_2O$ and 1.2 mmol (91.2 mg) of thiourea were dissolved in 2 mL ethylene glycol under ultrasonication. Then, the two solutions were mixed in a three-necked flask with 5 mg PVP. After the mixed system was refluxed at 110 °C for 10 min, the system was cooled to room temperature naturally. A black precipitate was obtained by centrifugation and washed with deionized water and ethanol several times to remove the impurities. Finally, the as-obtained product was dried under vacuum at 60 °C overnight for further characterization.

In order to investigate the influence of experimental parameters on the formation of Bi_2S_3 flowerlike superstructures, the above process was repeated. Each time, only one parameter was changed.

2.2 Characterization

The X-ray powder diffraction (XRD) patterns were obtained on a Shimadzu XRD-6000 X-ray diffractometer equipped with Cu Kα radiation (λ = 0.154060 nm), employing a scanning rate of 0.02° s^{-1} and 2θ ranges from 10° to 80°. TEM and HRTEM images of the product were obtained on a JEM-2100 high resolution transmission electron microscope, employing an accelerating voltage of 200 kV. SEM images and energy dispersive spectrometry (EDS) of the products were obtained on a Hitachi S-4800 field emission scanning electron microscope, employing an accelerating voltage of 5 kV and 15 kV, respectively. UV-vis absorption spectra were recorded on a Metash 6100 UV-vis absorption spectrophotometer (Shanghai). The Brunauer–Emmett–Teller (BET) specific surface area and BJH pore size were obtained on a Micromeritics ASAP 2050 instrument at liquid-nitrogen temperature using nitrogen gas as the adsorbate, in which all samples were previously degassed at 200 °C for 6 h in flowing N_2.

2.3 Catalytic study

To investigate the catalytic properties of the as-obtained Bi_2S_3 flowerlike microspheres for the reduction of some aromatic compounds including 4-nitroaniline, 4-nitrophenol, and 2-nitrophenol by $NaBH_4$, a series of solutions were freshly prepared before the experiments. In a typical process, appropriate amounts of organic compounds and the catalysts were firstly mixed in a small amount of distilled water. Then, a certain volume of $NaBH_4$ solution was introduced into the above system to form a 3 mL solution. Here, the concentrations of the organic compound, $NaBH_4$ and the catalyst were 0.5×10^{-4} mol L^{-1}, 2.0×10^{-2} mol L^{-1} and 50–150 mg L^{-1}, respectively. The reducing reaction processes were monitored using a Metash 6100 UV-vis spectrophotometer.

3. Results and discussion

3.1 Structural and morphology characterization

After $Bi(NO_3)_3{\cdot}5H_2O$ was dissolved in glycol, water molecules were freed from $Bi(NO_3)_3{\cdot}5H_2O$. These water molecules reacted with thiourea under the present oil-bath conditions to produce H_2S, which rapidly combined with Bi^{3+} ions to form Bi_2S_3. To prove the formation of Bi_2S_3 under the present oil-bath conditions, the XRD technology was employed for the phase analysis of the black precipitate. Upon comparison with the data of JCPDS card file no. 17-0320, all the diffraction peaks can be indexed as the orthorhombic Bi_2S_3 form (see Fig. 1a). Further evidence to form Bi_2S_3 came from the EDS analysis of the as-prepared product.

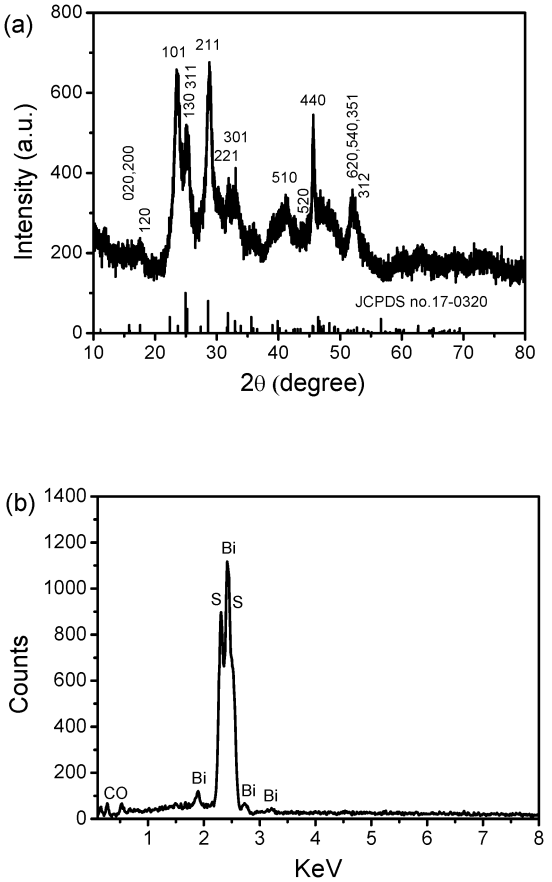

Fig. 1 (a) The XRD pattern and (b) EDS analysis of the product prepared by the present oil-bath route at 110 °C for 10 min.

As shown in Fig. 1b, strong Bi and S peaks are clearly visible. Based on the calculation of the peak areas, the molar ratio of Bi/S is very close to the stoichiometric ratio of Bi_2S_3. Moreover, the weak carbon and oxygen peaks should be attributed to the physical adsorption of the product to carbon and oxygen elements.

Fig. 2a shows a representative SEM image of the product. Abundant uniform flowerlike microspheres with ~2 μm in diameter can readily be seen. Further magnification indicated that the flowerlike microspheres were constructed by plentiful nanoneedles with a mean diameter of ~50 nm (Fig. 2b). This morphology is similar to a plant called *Echinops sphaerocephalus linn* in nature, which is one of Asteraceaes (see Fig. 2c). The above spherical flowerlike microstructures were further confirmed by TEM observation. As shown in Fig. 2d, the flowerlike microspheres with a mean size of 2 μm are visible. Prickly surfaces indicate that the flowerlike microspheres are constructed by plentiful nanoneedles, which are in good agreement with the results of SEM. A HRTEM image of a nanoneedle of the flowerlike microspheres is depicted in Fig. 2e. The clear stripes show good crystallinity of the product, and the distances between the two intersecting planes are measured to be about 0.50 nm and 0.37 nm, respectively, which correspond to the (120) and (101) planes of Bi_2S_3.[24] The above facts prove the formation of Bi_2S_3. Furthermore, the nitrogen adsorption–desorption experiments showed that the specific surface area of the flowerlike microspheres was 32.4 $m^2\ g^{-1}$ and the BJH pore width was ~9.4 nm (see Fig. 2f).

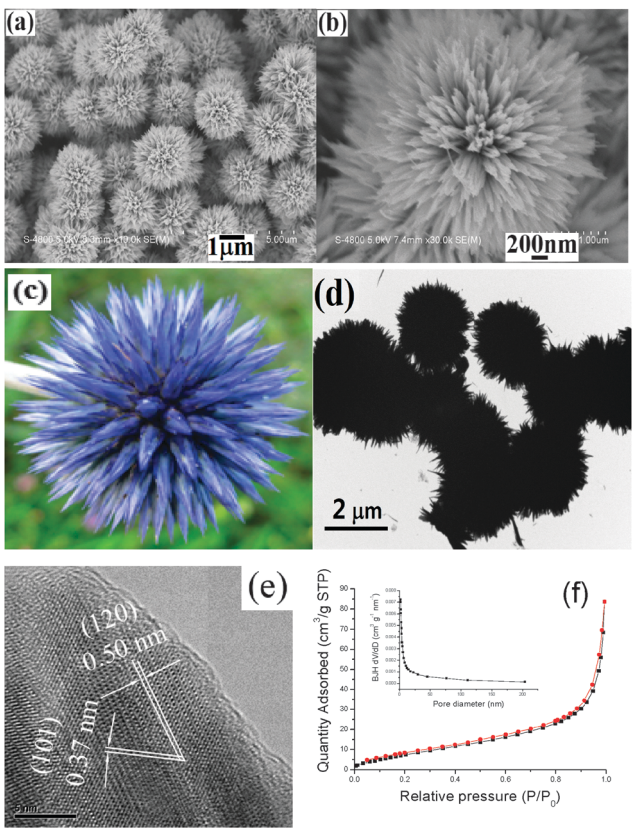

Fig. 2 (a) A representative low-magnification SEM image, (b) a high-magnification SEM image, (c) a photograph of *Echinops sphaerocephalus linn*, (d) a typical TEM image and (e) a HRTEM image of the product prepared by the present oil-bath route at 110 °C for 10 min. (f) N_2 adsorption–desorption curves of flowerlike Bi_2S_3 microstructures before and after using the catalyst. The inset in (f) is the relation plot of pore volume and pore diameter.

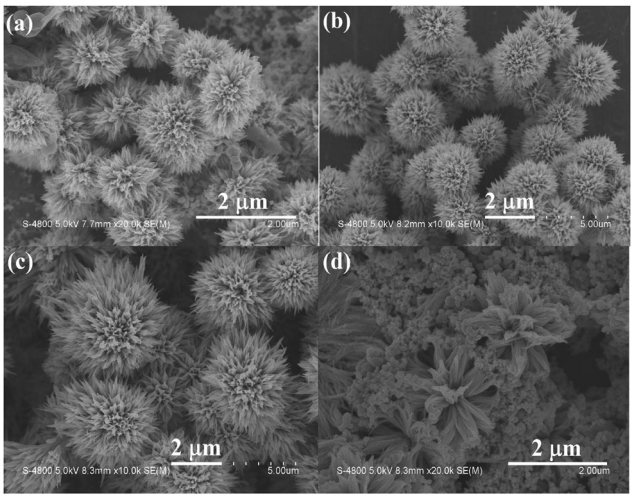

Fig. 3 SEM images of the products prepared at various reflux temperatures for 10 min: (a) 90 °C, (b) 100 °C, (c) 120 °C and (d) 130 °C.

Further investigations showed that the temperature and the surfactant played crucial roles in the formation of flowerlike Bi_2S_3 microspheres. As shown in Fig. 3a, when the reaction was completed at 90 °C for 10 min, the flowerlike microspheres had become the main product besides few small particles. Simultaneously, the sizes of flowerlike microspheres ranged from 1 to 2 μm. When the temperature of 100 °C was employed, small particles disappeared and the product completely consisted of the flowerlike microspheres with a mean diameter of ~2 μm (see Fig. 3b). Upon further raising the temperature to 120 °C, the flowerlike microspheres continuously grew up (see Fig. 3c). At 130 °C, however, abundant particulate products reappeared. At the same time, the flowerlike microspheres collapsed (Fig. 3d). Obviously, the optimum temperature range to prepare the flowerlike superstructures should be 100–120 °C.

Fig. 4 depicts the SEM images of the products prepared under the presence of various surfactants. As shown in Fig. 4a, when no surfactant was used in the system, the final product presented hierarchical microstructures with a large size and broad size distribution. After PVP was replaced by cetyltrimethylammonium bromide (CTAB) or sodium dodecyl benzene sulfonate (SDBS) with the same amount, porous structures constructed by abundant nanoplates or flowerlike microstructures built up of plentiful microrods were obtained, respectively (see Fig. 4b and c). Obviously, the present flowerlike microspheres could only be obtained under the assistance of PVP. It is well known that CTAB is a cationic surfactant and SDBS an anionic one. When CTAB and SDBS were separately used as surfactants, they could be repelled by Bi^{3+} ions or S^{2-} ions while PVP was not repelled due to its nonionic surfactant characteristics. Thus, the three surfactants had different influences on the shape control of the final product. Moreover, the amount of PVP could markedly affect the morphology of the final product.

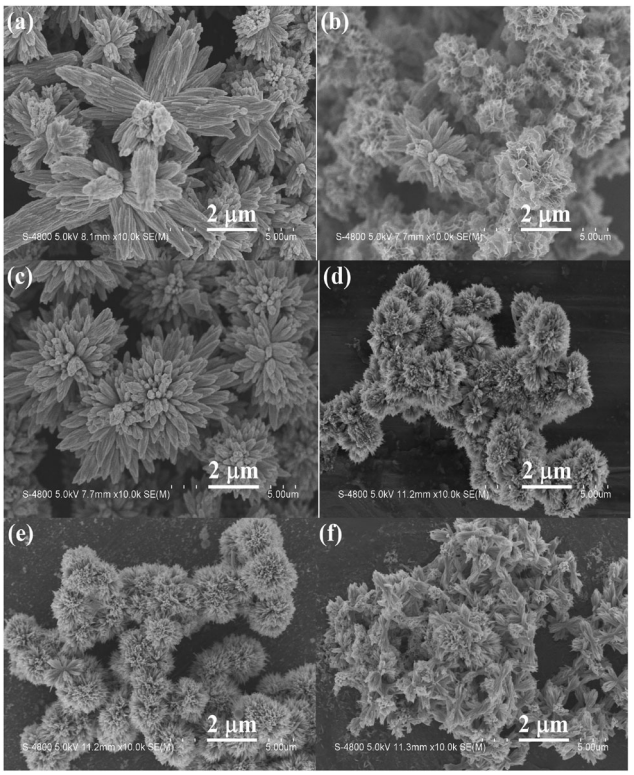

Fig. 4 SEM images of the products obtained at 110 °C for 10 min from the systems with various surfactants: (a) no surfactant, (b) 5 mg of CTAB, (c) 5 mg of SDBS, (d) 1.25 mg of PVP, (e) 2.5 mg of PVP and (f) 7.5 mg of PVP.

When 1.25 mg of PVP was employed, flowerlike structures constructed by nanorods could be obtained. However, they compactly connected with each other and no discrete flowerlike microspheres were formed (see Fig. 4d). However when 2.5 mg of PVP was used, flowerlike microspheres could easily be distinguished although the connection among flowerlike structures still existed (Fig. 4e). When the amount of PVP was increased to 5 mg, discrete and uniform flowerlike microspheres were formed (Fig. 2a). Upon further increasing the amount of PVP to 7.5 mg, however, the flowerlike microspheres were destroyed (Fig. 4f). The above facts imply that excess PVP is unfavorable for the formation of flowerlike microspheres. In the present work, PVP had two roles in the formation of Bi_2S_3 flowerlike microspheres: the structure-directing reagent and surfactant. When small amounts of PVP existed in the system, they could adsorb on some specific crystal surfaces of the nuclei of a preferred crystalline phase in the initial nucleation stage. Subsequently, the nuclei grew only along the directions unoccupied by PVP.[25] Thus, discrete and uniform flowerlike microspheres gradually formed with the increasing PVP amount to 5 mg. Here, PVP mainly acted as the structure-directing reagent. When excess PVP was employed, however, the surfactant function of PVP predominated, causing the destruction of the flowerlike microspheres.

3.2 Application in the catalytic reduction of 4-nitroaniline

In recent years, the reduction of aromatic nitrocompounds by sodium borohydride ($NaBH_4$) in the aqueous solution has made great progress.[22,26] Many inorganic compounds micro/nanostructures were found to have strong catalytic activity, including metals, oxides and phosphides. One of the aromatic nitrocompounds 4-nitroaniline can be reduced to 1,4-phenylenediamine (1,4-PD), which is an important intermediate to prepare dyes, curing agents for epoxy resin and rubber antioxidants.[27–29] As mentioned in the previous section, nanostructural Bi_2S_3 was mainly used as photoresponse and field emission materials,[10] electrochemical hydrogen storage devices,[11,12] photocatalysts,[13–15] and electrode materials in lithium ion battery.[16] To date, no report has been found to evidence its use as a catalyst for the reduction of aromatic nitrocompounds by $NaBH_4$ in aqueous solutions. In the present work, experiments exhibited that the as-obtained flowerlike Bi_2S_3 microspheres showed an excellent catalytic activity for the reduction of some aromatic nitrocompounds by $NaBH_4$ in aqueous systems, including 4-nitroaniline (4-NA). Fig. 5a shows the UV-vis absorption spectra of the 4-NA–$NaBH_4$ system in the presence of 100 mg L^{-1} catalyst at various reaction duration. A strong absorption peak at 380 nm, which originated from the intermediate formed by 4-NA and $NaBH_4$,[30] gradually decreased with increase in the reaction duration. Simultaneously, a new peak at 306 nm appeared, which belonged to the characteristic absorption peak of 1,4-PD.[29] After reacting for 9 min, the peak at 380 nm almost disappeared, indicating that the reduction of 4-NA had closely completed. It is worth noting that the reduction rate was very rapid at the initial stage of the reaction, indicating that no inducing period existed in the current reductive reaction in the presence of Bi_2S_3 catalyst. Subsequently, the reaction rate gradually slowed down due to the consumption of reactants. Fig. 5b depicts the correlation between the reaction rate and the amount of the catalyst. Obviously, the reductive reaction can be promoted by increasing the amount of the catalyst from 50, 100 to 150 mg L^{-1}. Furthermore, the present catalyst could be recycled by centrifugation and repeated washing. As shown in Fig. 5c, after the catalyst was used four times, its catalytic efficiency could still reach 67% within 9 min. Compared with the first catalytic efficiency, however, the catalytic ability of the catalyst had markedly decreased. This should be attributed to the shape change of the catalyst. As seen from Fig. 5d, the surfaces of the flowerlike microspheres became compact than those shown in Fig. 2a. Namely, the shape of the catalyst had retrograded after the first cycle. Here, the specific surface area and the BJH pore width of the catalyst changed to 28.7 $m^2\ g^{-1}$ and $\sim$10.6 nm, respectively (see Fig. 2f). Hereafter, the shape of the catalyst hardly changed, and so the catalyst presented the close catalytic capacity from the 2nd to the 4th reduction. In a catalytic system, usually, the catalytic activity of a catalyst is mainly determined by its active site number. More the active sites are, more the reactant molecules adsorbed and, thus, higher the catalytic efficiency of the catalyst is. Since the catalyst with a large specific surface area often has more active sites, its catalytic efficiency will be higher than that of the one with a small specific surface area. In the present work, the shape retrogradation of the catalyst after the 1st cycle caused the decrease of the specific surface area. As a result, the active sites of the catalyst reduced. This led to the decrease in the catalytic efficiency of the catalyst after the 1st cycle.

From Fig. 3 and 4, it is evident that the morphology of Bi_2S_3 can be affected by the reaction temperature and the surfactant.

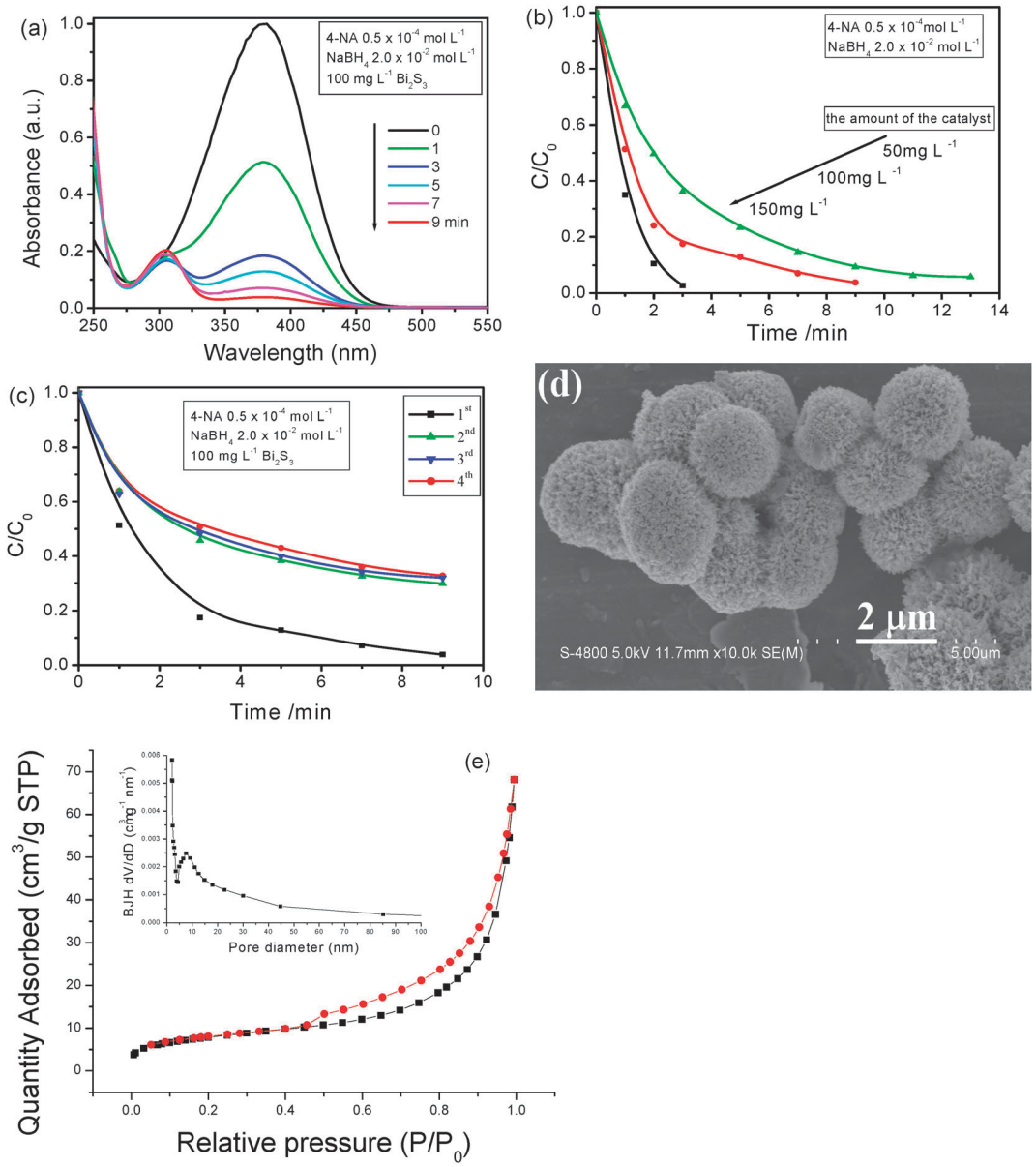

Fig. 5 (a) UV-Vis absorption spectra of the 4-NA–$NaBH_4$ system in the presence of 100 mg L Bi_2S_3 flowerlike superstructures for various reaction duration; (b) the influence of the original amount of the catalyst on the reduction of 4-NA; (c) cycle times of the catalyst. (d) SEM image and (e) N_2 adsorption–desorption curves of the catalyst after the first cycle. The inset in (e) is the relation plot of pore volume and pore diameter.

In contrast, therefore, we also investigated the catalytic activities of Bi_2S_3 with various shapes. Fig. 6a and b depict the UV-Vis absorption spectra of the 4-NA–$NaBH_4$ system in the presence of 100 mg L^{-1} Bi_2S_3 prepared from the same system at different temperatures and under the assistance of various surfactants at 110 °C for 10 min, respectively. As shown in Fig. 6a, the catalytic efficiencies of the catalysts prepared at different temperatures for 10 min are in turn 35% (130 °C), 65% (90 °C), 74% (120 °C), 81% (100 °C) and 96% (110 °C). The product prepared at 130 °C exhibits the weakest catalytic activity, which should be attributed to the morphology retrogression of flowerlike Bi_2S_3 microspheres (see Fig. 3d). Similarly, when the products prepared separately from the systems containing SDBS and CTAB were used as the catalysts, the catalytic efficiencies also markedly decreased (see Fig. 6b).

Moreover, further investigations discovered that the as-obtained flowerlike Bi_2S_3 microspheres could also catalyze the reduction of other aromatic nitro compounds, such 4-nitrophenol (4-NP) and 2-nitrophenol (2-NP), under the same experimental conditions. However, the reducing rate of 2-NP was much faster than that of 4-NP in the presence of the same amount of the catalyst (see Fig. 7). Owing to keeping the other conditions unchanged, the above difference in the reaction rates should be related to the molecular structures of organic compounds.

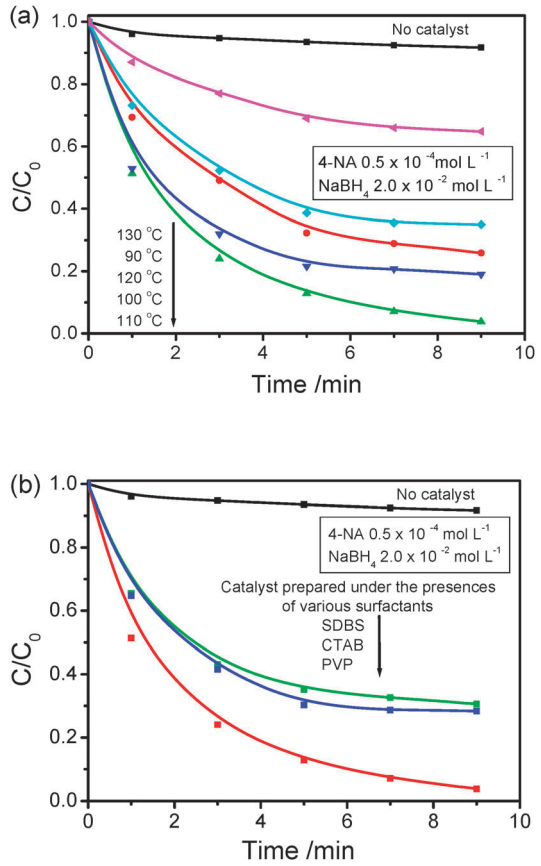

Fig. 6 UV-Vis absorption spectra of the 4-NA–$NaBH_4$ system in the presences of Bi_2S_3 with various shapes prepared at different temperatures (a) or under the assistances of various surfactants (b).

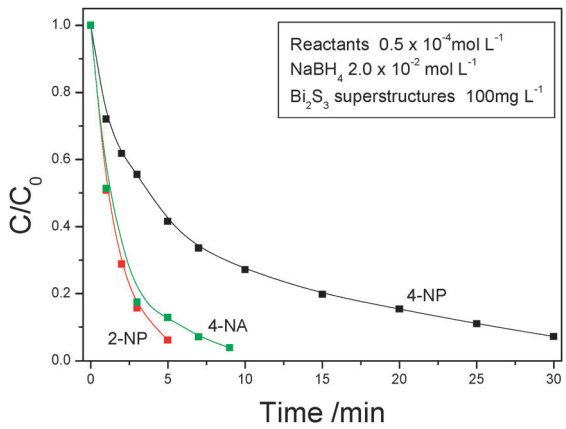

Fig. 7 The concentration–time curves of various aromatic nitro compounds under the same experimental conditions.

4. Conclusions

In summary, flowerlike Bi_2S_3 microspheres have been successfully synthesized *via* a facile and rapid oil-bath route at 110 °C for 10 min in the presence of PVP. The experiments showed that the optimum temperature to form flowerlike Bi_2S_3 microspheres ranged from 100 to 120 °C, and that PVP played a crucial role in the formation of flowerlike Bi_2S_3 microspheres. However, excess PVP was unfavorable for the formation of flowerlike Bi_2S_3 microspheres. It was also evidenced from the experiments that Bi_2S_3 with various shapes could be utilized as catalysts for the reduction of 4-nitroaniline in excess $NaBH_4$ aqueous solutions. Among them, the flowerlike Bi_2S_3 superstructures presented the best catalytic activity. Furthermore, the flowerlike Bi_2S_3 superstructures could also catalyze the reduction of some other aromatic nitro compounds including 4-nitrophenol and 2-nitrophenol in $NaBH_4$ aqueous solutions. The present work provides a new catalyst choice in industry for the reduction of the above mentioned aromatic nitro compounds in $NaBH_4$ aqueous solution.

Acknowledgements

The authors thank the National Natural Science Foundation of China (21171005) and Key Foundation of Chinese Ministry of Education (210098) for the financial support.

References

1 C. H. Lai, M. Y. Lu and L. J. Chen, *J. Mater. Chem.*, 2012, **22**, 19.
2 Y. Wu, C. Wadia, W. L. Ma, B. Sadtler and A. P. Alivisatos, *Nano Lett.*, 2008, **8**, 2551.
3 T. L. Li, Y. L. Lee and H. Teng, *J. Mater. Chem.*, 2011, **21**, 5089.
4 M. J. Bierman and S. Jin, *Energy Environ. Sci.*, 2009, **2**, 1050.
5 D. D. Miller and A. Heller, *Nature*, 1976, **262**, 280.
6 J. Grigas, E. Talik and V. Lazauskas, *Phys. Status Solidi B*, 2002, **232**, 220.
7 L. J. Farrugia, F. J. Lawlor and N. C. Norman, *Polyhedron*, 1995, **14**, 311.
8 R. S. Mane, B. R. Sankapal and C. D. Lokhande, *Mater. Chem. Phys.*, 1999, **60**, 196.
9 O. Rabin, J. M. Perez, J. Grimm, G. Wojtkiewicz and R. Weissleder, *Nat. Mater.*, 2006, **5**, 118.
10 X. L. Yu and C. B. Cao, *Cryst. Growth Des.*, 2008, **8**, 3951.
11 B. Zhang, X. C. Ye, W. Y. Hou, Y. Zhao and Y. Xie, *J. Phys. Chem. B*, 2006, **110**, 8978.
12 L. S. Li, N. J. Sun, Y. Y. Huang, Y. Qin, N. N. Zhao, J. N. Gao, M. X. Li, H. H. Zhou and L. M. Qi, *Adv. Funct. Mater.*, 2008, **18**, 1194.
13 T. Wu, X. G. Zhou, H. Zhang and X. H. Zhong, *Nano Res.*, 2010, **3**, 379.
14 F. J. Chen, Y. L. Cao and D. Z. Jia, *J. Colloid Interface Sci.*, 2013, **404**, 110.
15 G. Konstantatos, L. Levina, J. Tang and E. H. Sargent, *Nano Lett.*, 2008, **8**, 4002.
16 J. M. Ma, J. Q. Yang, L. F. Jiao, T. H. Wang, J. B. Lian, X. C. Duan and W. J. Zheng, *Dalton Trans.*, 2011, **40**, 10100.
17 (*a*) C. V. Rode, M. J. Vaidya, R. Jaganathan and R. V. Chaudhari, *Chem. Eng. Sci.*, 2001, **56**, 1299; (*b*) T. Komatsu and T. Hirose, *Appl. Catal., A*, 2004, **276**, 95; (*c*) C. V. Rode, M. J. Vaidya and R. V. Chaudhari, *Org. Process Res. Dev.*, 1999, **3**, 465.

18 (*a*) S. Saha, A. Pal, S. Kundu, S. Basu and T. Pal, *Langmuir*, 2010, **26**, 2885; (*b*) J. Zeng, Q. Zhang, J. Y. Chen and Y. N. Xia, *Nano Lett.*, 2010, **10**, 30; (*c*) F. Ke, J. F. Zhu, L. G. Qiu and X. Jiang, *Chem. Commun.*, 2013, **49**, 1267.
19 N. Sahiner, H. Ozay, O. Ozay and N. Aktas, *Appl. Catal., A*, 2010, **385**, 201.
20 Z. W. Seh, S. H. Liu and M. Y. Han, *Chem. – Asian J.*, 2012, **7**, 2174.
21 K. L. Wu, X. W. Wei, X. M. Zhou, D. H. Wu, X. W. Liu, Y. Ye and Q. Wang, *J. Phys. Chem. C*, 2011, **115**, 16268.
22 F. F. Yuan, Y. H. Ni, L. Zhang, S. M. Yuan and J. D. Wei, *J. Mater. Chem. A*, 2013, **1**, 8438.
23 J. D. Wei, Y. H. Ni, N. N. Xiang, Y. X. Zhang and X. Ma, *CrystEngComm*, 2014, **16**, 2113.
24 Z. P. Liu, S. Peng, Q. Xie, Z. K. Hu, Y. Yang, S. Y. Zhang and Y. T. Qian, *Adv. Mater.*, 2003, **15**, 936.
25 Z. Chen and M. H. Cao, *Mater. Res. Bull.*, 2011, **46**, 555.
26 G. W. Zhan, Y. L. Hong, F. F. Lu, A. R. Ibrahim, M. M. Du, D. H. Sun, J. L. Huang, Q. B. Li and J. Li, *Chem. Eng. J.*, 2012, **187**, 232.
27 C. Franco, *Eur. Polym. J.*, 1996, **32**, 43.
28 I. Yoshiaki and K. J. Masa-aki, *Health Sci.*, 2000, **46**, 467.
29 H. S. Lee and Y. W. Lin, *Ann. Occup. Hygg.*, 2009, **53**, 289.
30 V. Reddy, R. S. Torati, S. J. Oh and C. G. Kim, *Ind. Eng. Chem. Res.*, 2013, **52**, 556.

